Transport in nearly-free-electron metals. II. Phonon-limited relaxation time at high temperature*

H. B. Huntington
Department of Physics, Rensselaer Polytechnic Institute, Troy, New York 12181
and Laboratory for Atomic and Solid State Physics,† Cornell University, Ithaca, New York 14850

W.-C. Chan ‡
Department of Physics, Rensselaer Polytechnic Institute, Troy, New York 12181
(Received 30 April 1975)

The problem of electron transport at high temperatures has been attacked for a model divalent metal, using principally a two-plane-wave approximation and taking into account the Fermi-surface distortion. The electron mean free path is found as a function of position on the Fermi surface for phonon scattering only. The limiting high-temperature form of phonon-scattering structure factor is used and the effective electron-relaxation time is found by a somewhat novel iteration scheme that converges rapidly. Without loss of generality the electric field is chosen to act along a symmetry direction of the lattice. For the purpose of this application the phonon dispersion and anisotropy are disregarded. Simple consideration of two sets of Brillouin zones shows that their effects can be roughly superimposed for the usual nearly-free-electron metal. For a reasonably chosen set of material parameters the calculated dependence of electron relaxation time as a function of $\vec{k}$ is used to find the conductivity.

I. INTRODUCTION

The problem of electron-phonon interaction is central to a large part of metal physics. It plays a crucial role in the understanding of transport processes and has been extensively treated in the standard texts in this area.[1] The treatment is based on a linearized Boltzmann equation where the collision terms are given by the transition probabilities of time-dependent perturbation theory and both the lattice potential and the dynamics of the lattice elements are involved in the interaction. In addition to the applications to the theory of transport for electric charge and thermal energy, the electron-phonon interaction determines the strength of the pair binding for superconductivity and alters the effective electron mass.[2]

Although in the early stages of development there was a tendency to pass over detailed consideration of umklapp processes, careful work has shown their influence to be large even for monovalent metals[3] and to dominate the normal processes for polyvalent metals.[4] It greatly increases the magnitude of the scattering and at low temperature can alter the temperature dependence of the Grüneisen prediction (T^5 for resistivity) and enhance the departure from Matthiessen's rule in situations involving the breakdown of the relaxation-time approximation.[5]

For the lattice potential as seen by the electrons it has been customary to employ suitable pseudopotentials or, more directly, their transforms.[6] The lattice dynamics are usually treated in the one-phonon approximation,[7] although Baym[8] has shown that the complete complexity of the phonon influence, including multiphonon processes and the Debye-Waller factor, can be incorporated by working directly with the time-correlation transforms of the scattering of slow neutrons. It appears that the application of this sort of broader technique has been limited so far to liquid metals.[9]

Recently there have been several detailed calculations of transport properties in polyvalent metals. These include the work of Dynes and Carbotte[4] on Na, K, Al, and Pb and of Borchi, DeGennaro, and Taselli[10] on the hexagonal metals, Be, Mg, and Zn averaged over crystal orientation, i.e., appropriate to polycrystals. Studies of the anisotropy of resistivity for the hexagonal metals have been carried on by Pecheur and Toussaint.[11] The latter have also explored[12] anisotropy of thermal resistivity in these metals. In all these cases the solution of the Boltzmann equation proceeded from the variational procedure,[13] which gives presumably good upper limits to the resistivities, but little information on the variation of the relaxation time over the Fermi surface. For the applications to specific metals the variations of the Fermi surface from a sphere were generally disregarded as well as the coupling between orthogonalized-plane-wave (OPW) functions.

In this paper the emphasis is somewhat different in that we have concentrated on the influence of electron coupling through the pseudopotential components and used in general a two-plane-wave approximation. Also because we were interested in the variation of the relaxation time over the Fermi surface, we have employed an iteration-type solution to the Boltzmann equation instead of the more elegant variational procedure. This iteration pro-

cedure is appreciably different from what has been used in earlier treatments.[14] The direct investigation of the relaxation time should be useful in evaluating other transport effects. In this respect we are particularly concerned with electromigration or the mass transport in metal under the influence of high electric currents. Here the "electron wind" effect is important and depends directly on the electron mean free path. The anisotropy of this effect in noncubic metals[15] has been rather a mystery and the knowledge of the anisotropy of the electron relaxation time is an important clue to its understanding.

To simplify the geometry the calculation has been applied to a fictitious metal with a simple-cubic structure and two electrons per atom. The resulting zone structure gives rather well separated zone interactions so that it is generally sufficient as a first approximation to consider only one coupling interaction as an reasonable approximation. To simplify the surface integrations the form factor is expressed as a series in the square of the scattering vector.

Section II of this paper displays the basic formalism of the approach. Section III applies the method to the simplest of the umklapp processes. In Sec. IV we consider the generalization to the more complex electron coupling. In Sec. V we show how to combine all contributions to the obtaining of the relaxation time and give a simple example of the application. Section VI is the concluding section.

II. BASIC FORMALISM–BOLTZMANN EQUATION

The investigation of the electron mean free path $\lambda(k)$, over the Fermi surface when limited by phonon scattering, begins with the Boltzmann equation for the conductor in the uniform electric field E,

$$\left(-\frac{\partial f_0}{\partial \epsilon}\right)\vec{v}(\vec{k})\cdot e\vec{E}=\sum_{k'}\frac{2\pi}{\hbar}\,|M(\vec{k},\vec{k}',\vec{q},j)|^2 \times\delta(\epsilon_k-\epsilon_{k'}+h\omega_{qj})\{N_{\vec{q}j}f(\vec{k})[1-f(\vec{k}')] - N^+_{\vec{q}j}f(\vec{k}')[1-f(\vec{k})]\} + [\text{analogous terms involving } \delta(\epsilon_{\vec{k}}-\epsilon_{\vec{k}'}-h\omega_{\vec{q}j})]. \tag{2.1}$$

The left-hand side is the usual drift term in the momentum coordinates in a force field eE and on the right-hand side are the scattering terms calculated according to the standard equations of second-order perturbation theory. The M quantity is the interaction matrix element which induces a transition between electron states $\vec{k}$ and $\vec{k}'$ with the creation or annihilation of a phonon of wave vector $\vec{q}$ and polarization j. The symbols for electron energy and velocity are ϵ and $\vec{v}$, respectively, and ω is the phonon frequency. The first term in the curly brackets represents phonon annihilation and the second term the phonon creation. The N_q is the initial phonon distribution and the N_q^+ is the distribution after the creation of the phonon. The f is the electron distribution and f_0 is the equilibrium (Fermi-Dirac) distribution.

For the high-temperature region one can assume phonon equilibrium so that

$$N_q=N_q^+-1\simeq N_q^+ . \tag{2.2}$$

For the electron distributions we write $f-f_0=g$ so that one can linearize the Boltzmann equation by setting

$$g(\vec{k})=-\left(\frac{df_0}{d\epsilon}\right)e\vec{E}\cdot\vec{\lambda}(\vec{k}) , \tag{2.3}$$

where $\vec{\lambda}(\vec{k})$ is the electron mean free path between scatterings.

Changing the summation to an integration one can now rewrite the Boltzmann equation (2.1) as

$$\vec{v}(\vec{k})=2\left(\frac{V}{8\pi^3}\right)\int[\vec{\lambda}(\vec{k})-\vec{\lambda}(\vec{k}')]\,W(\vec{k},\vec{k}')\,d\vec{k}' . \tag{2.4}$$

Here the $W(k, k')$ is the transition probability for the electron to go from state k to k' with no implicit dependence on the phonon density. The factor of 2 arises from the small size of $h\omega$ which makes the two parts of Eq. (2.1) equivalent. Again from time-dependent perturbation one has

$$W(\vec{k},\vec{k}')=(2\pi/\hbar)\,|\langle k|V_s|k'\rangle|^2\,\delta(\epsilon(\vec{k})-\epsilon(\vec{k}')) , \tag{2.5}$$

where V_s is the potential responsible for electrons scattering from state $\vec{k}$ to $\vec{k}'$.

Our variational approach starts by selecting a particular direction, usually a symmetry axis, along which the electric field acts. For each electron state there is defined a relaxation time

$$\tau_p(\vec{k})=\lambda_p(\vec{k})/v_p(\vec{k}) , \tag{2.6}$$

where λ_p and v_p are the components of $\vec{\lambda}$ and $\vec{v}$ in the fixed direction p. It should be emphasized that the tensor property of τ is sacrificed in this definition, but this is not too inconvenient. We determine $\tau_p(\vec{k})$ from a series

$$\tau_p(\vec{k})=\sum_{i=1}\tau_{pi}(\vec{k}) \tag{2.7}$$

by an iteration scheme based on the assumption that τ is not a rapidly varying function of $\vec{k}$. The leading term $\tau_{p1}(\vec{k})$ is determined on the basis that τ is sufficiently constant to be taken out from the integral in Eq. (2.4). (This starting approximation has also been suggested by Ziman[13] and Taylor.[14]) We have

$$\tau_{p1}(\vec{k})=v_p(\vec{k})/A(\vec{k}) , \tag{2.8}$$

where

$$A(\vec{k}) = \frac{V}{4\pi^3} \int [v(\vec{k}) - v(\vec{k}')] W(\vec{k}, \vec{k}')\, d\vec{k}' \,. \quad (2.9)$$

Substitution of Eq. (2.8) into Eq. (2.4) leads to

$$0 = \int [\tau_{p1}(\vec{k}) - \tau_{p1}(\vec{k}')]\, v(\vec{k}')\, W(\vec{k}, \vec{k}')\, d\vec{k}' + \int \sum_{n=2} [\tau_{pn}(\vec{k}) v(\vec{k}) - \tau_{pn}(\vec{k}') v(\vec{k}')] W(\vec{k}, \vec{k}')\, d\vec{k}' \,. \quad (2.10)$$

The next approximation is

$$\tau_{p2}(\vec{k}) = \int [\tau_{p1}(\vec{k}') - \tau_{p1}(\vec{k})] v(\vec{k}') \times W(\vec{k}, \vec{k}')\, d\vec{k}' [A(\vec{k})]^{-1} \,, \quad (2.11)$$

and successively

$$\tau_{p,n+1}(\vec{k}) = \int [\tau_{pn}(\vec{k}') - \tau_{pn}(\vec{k})]\, v(\vec{k}') \times W(\vec{k}, \vec{k}')\, d\vec{k}' [A(\vec{k})]^{-1} \,. \quad (2.12)$$

This iteration appears in general to converge rapidly. The formal conditions for convergence will be considered in the succeeding paper.[16]

For a pure metal, one can write the matrix elements of the scattering potential $\langle \vec{k} | V_s | \vec{k} \rangle$ as the product of a form factor $F(\vec{k} - \vec{k}')$ which is the transform of the pseudopotential of the lattice atom and the structure factor of the lattice. In the standard treatment of phonon scattering[7] the structure factor is expanded in terms of the phonon waves. For single-phonon scattering the matrix element is proportional to the phonon amplitude and one obtains

$$|\langle \vec{k} | V_s | \vec{k}' \rangle|^2 = (2N)^{-1} \sum_\sigma |a_{q\sigma}|^2 (\vec{\kappa} \cdot \vec{e}_{q\sigma})^2 |F(\vec{\kappa})^2|^2 \,, \quad (2.13)$$

where $a_{q\sigma}$ and $e_{q\sigma}$ are the amplitude and polarization, respectively, of the phonon with wave number $\vec{q}$ and polarization index σ. The initial factor of $\frac{1}{2}$ occurs in Eq. (2.13) because only one scattering process (phonon creation *or* annihilation) is involved. The scattering vector is $\vec{\kappa} = \vec{k} - \vec{k}'$. The conservation of crystal momentum requires that $\vec{\kappa} = \vec{q} + \vec{Q}$, the (annihilated) phonon wave number, where $\vec{Q}$ is 2π times a translational vector of the reciprocal lattice. The umklapp processes are characterized by $\vec{Q} \neq 0$. For our interests we can replace $|a(\vec{q})|^2$ by its high-temperature approximation,[7]

$$a_q^2 = kT/M\omega_q^2 \,, \quad (2.14)$$

where k is Boltzmann's constant, T is the absolute temperature, M is the mass of the metal atom, and ω_q is the angular frequency of the phonon wave. For the normal processes ($\vec{Q} = 0$) only longitudinal waves are involved, $\vec{\kappa} = (\vec{q})$, and Eq. (2.13) on the right-hand side reduces to $(kT/2Mc_l^2)|F(\vec{q})|^2$, where c_l is the longitudinal sound velocity. For metals, however, not all the Fermi surface can be spanned with normal processes and umklapp is involved. Where it is, the shear waves are important.

Because of our interest in the effect of the Brillouin-zone (BZ) intersections, we have chosen in this investigation to deal with a fictitious metal having a simple-cubic structure and two electrons per atom, as mentioned in Sec. I. Choosing to work in the extended zone scheme, we visualize a nearly spherical Fermi surface intersected by the three mutually perpendicular BZ's. Without loss of generality, we take the electric field $\vec{E}$ along the Z axis and put $\vec{k}$ in the upper hemisphere. With $\vec{k}$ as an origin we construct a phonon space, and as shown in Fig. 1(a) mark off the cell structure into which the phonon zone planes divide the Fermi surface for integration over k' [Fig. 1(b)].

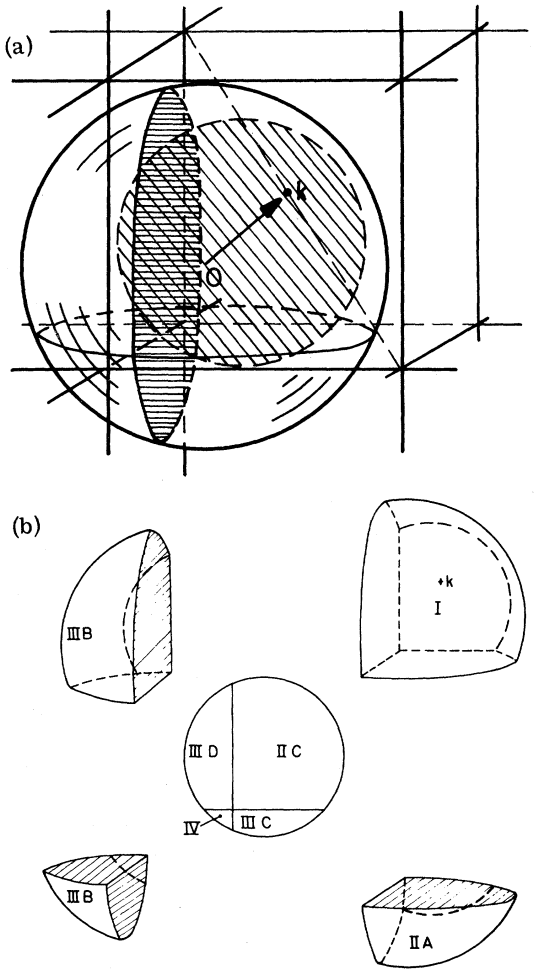

FIG. 1. (a) Fermi surface intersected by various phonon planes and (b) exploded view of resulting cell structure.

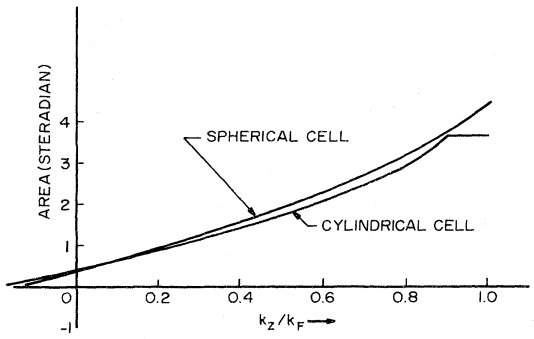

FIG. 2. Comparison of enclosed surfaces for the spherical and cylindrical phonon cells, respectively, in cell IIA as a function of k_z/k_F.

The nomenclature is to call the central cell in which $\vec{k}$ appears I and the three cells that adjoin I are called IIA, IIB, and IIC reserving IIA for the region to the $-Z$ side of I. The next more distant cells, each of which share an edge with I, are called IIIB, IIIC, and IIID and there is even a small cell IV with common corner with I.

Of course these BZ's are cubes, but since the intersection of cube and sphere is complicated by two orientation angles, we were constrained to approximate the zone first by a sphere and in later considerations by a cylinder with altitude equal to the cube edge. Both approximations have their individual uses and the added symmetry allows in each case that one variable in the surface integration in Eq. (2.4) be done analytically as in Sec. III. We shall also see that both approximations are quite mutually consistent. For example, we see in Fig. 2 plots comparing the amount of enclosed surface in cell IIA as a function of the k projection along the Z axis for both sphere and cylinder models of the phonon cell; the consistency is apparent.

For $\vec{k}$ on the BZ itself the possibility for $\vec{Q}=\vec{\kappa}$ and $\vec{q}=0$ exists, in which case $|\langle k|V_s|k'\rangle|^2$ [Eq. (2.13)] appears to go infinite—a situation frequently referred as a "hot spot" on the Fermi surface. Actually a more careful study will show that the infinity does not really occur when one considers the Bragg coupling for the electrons and the deformation of the Fermi surface (see Sec. III).

As long as only single-plane-wave functions are used for the electrons, a particular choice for $\vec{\kappa}$ determines $\vec{q}$ and $\vec{Q}$ uniquely. However, once Bloch wave functions are used, the possibility for Bragg diffraction presents multiple choices for Q; this is particularly important for those states near the BZ. Then for a given κ there may be three or four values for $\vec{\kappa}+\vec{K}$ that replace κ in Eq. (2.13) giving rise to separate terms. Here $\vec{K}$ is like $\vec{Q}$, 2π times a translational vector of the reciprocal lattice, but introduced by Bragg diffraction rather than by umklapp. To treat this complication the electron zone structure must be specified in addition to the phonon structure.

In accord with the basic assumption of the nearly-free-electron metal (NFEM) that the zone energy gaps are small, we treat the Bragg coupling of the various zones by superposition only, maintaining that those regions where superposition might break down (near edges and corners of the zone structure) are relatively unimportant. Consequently, two-plane-wave functions suffice quite generally for the appropriate Bloch functions for the electrons throughout most of the Fermi surface. They have the standard form,

$$\psi_k(r)=V^{-1/2}[\alpha(\mu)\,e^{i\vec{k}\cdot\vec{r}}+\beta(\mu)\,e^{i(\vec{k}+\vec{K})\cdot\vec{r}}]\,, \qquad (2.15)$$

where α and β are given by

$$\alpha=(\tfrac{1}{2}\{1+|\gamma-\mu|[(\gamma-\mu)^2+g^2]^{-1/2}\})^{1/2}\,, \qquad (2.16a)$$

$$\beta=\pm(\tfrac{1}{2}\{1-|\gamma-\mu|[(\gamma-\mu)^2+g^2]^{-1/2}\})^{1/2}\,. \qquad (2.16b)$$

Here the components of $\vec{k}$ parallel and perpendicular to $\vec{K}$ are written $k_{\parallel}=\mu k_F$ and $k_{\perp}=\nu k_F$, respectively, (k_F is the radius of the undistorted Fermi sphere). Let $\mu=\gamma=K/2k_F$ specify the location of the BZ. The parameter g which determines the band gap splitting is $V(\vec{K})/2\epsilon_F\gamma$, where ϵ_F is the Fermi energy and $V(\vec{K})$ is the Kth component of the lattice potential. In this work we shall take $V(\vec{K})$ to result from a purely local potential and to be equal to $F(\vec{K})$, the atomic form factor. Strictly this holds only at absolute zero and $V(K)$ should be multiplied by the square root of the Debye-Waller factor for $T>0$. For the electron energy near the Kth zone, we have

$$\epsilon/\epsilon_F=(k/k_F)^2+2\gamma\{\gamma-\mu\pm[(\gamma-\mu)^2+g^2]^{1/2}\}\,. \qquad (2.17)$$

The plus sign in Eq. (2.17) goes with $\mu>\gamma$. The sign of β in Eq. (2.16) is the same as $F(K)$ for $\mu>\gamma$ and reverses for $\mu<\gamma$. For this model the electron velocity appearing in Eq. (2.1) is given by $\vec{v}=\hbar^{-1}\vec{\nabla}_k\epsilon\cong\hbar\vec{k}/m^*$ except near a BZ, where the parallel component of $\vec{v}$ is altered. (m^* is the electron mass characteristic of the conduction band far from a BZ.) In general

$$v\simeq(\hbar k_f\mu/m^*)[1-2\beta_K(k)]\,. \qquad (2.18)$$

The choice of an analytic form for $F(\kappa)$ to be a power series in κ^2 has the double advantage that the fitting for small κ^2 is easy and that integration over one angular variable of the Fermi surface can be done analytically. In this work we have used a linear expression,

$$F(\kappa)=F_0[1-(1/2b)(\kappa/k_F)^2]\,, \qquad (2.19)$$

similar to that used by Feit and Huntington.[17] Here F_0 can, in general, be taken as a constant, $-\frac{2}{3}\epsilon_F$,

and b is a parameter which essentially determines the zero for $F(\kappa)$. For some metals such an expression can be made to give a reasonably good fit; for most a quadratic term would be preferable to give good fitting in the region around $\kappa = 2k_F$.

Before proceeding in Sec. III to the actual calculations, with this model, it is worthwhile to list briefly the shortcomings and assumptions of the approach and comment whether each is basic to the model, tractable by a more detailed procedure, or simply trivial: (a) The most serious shortcoming of the approach seems to be the neglect of the multiple phonon processes, especially since there seems no easy way to estimate their influence particularly at high temperature. (b) The method assumes that $F(\vec{\kappa}+\vec{K})$ is a function only of the magnitude of its argument. This is satisfactory for a local pseudopotential, but for a nonlocal pseudopotential it holds only if $\vec{\kappa}+\vec{K}$ connects states of the same energy. For some $\vec{K}$ this may not be even approximately true. (c) As will become evident, the phonon spectrum will be treated rather cavalierly since both dispersion and anisotropy are neglected in this treatment. However, the effects of these omissions can be estimated, and if need be, a more detailed treatment could take them into account.[16] (d) As mentioned above, a careful treatment for most metals will require an expression for F quadratic in κ^2 rather than linear as developed here. (e) Lastly, the use of spherical or cylindrical phonon zones appears to introduce relatively negligible error.

III. EVALUATION OF THE SCATTERING INTEGRALS FOR CELLS I AND II

In this section we shall proceed to evaluate certain integrals that pertain to cells I and II and that will be useful in constructing the complete $A(\vec{k})$ in Sec. IV. These integrals are

$$ {}_0m_C = \int_C p(\vec{k},\vec{k}')\,dS'/|\nabla_{k'}\epsilon| \,, \tag{3.1a} $$

$$ {}_{\parallel}m_C = \int_C \mu'[1-2\beta_K^2(k')]\,p(\vec{k},\vec{k}')\,dS'/|\nabla_{k'}\epsilon| \,, \tag{3.1b} $$

$$ {}_{\perp}m_C = \int_C \nu'\cos\phi\, p(\vec{k},\vec{k}')\,dS'/|\nabla_{k'}\epsilon| \,. \tag{3.1c} $$

Here C is the cell index, $\nu^2 = 1-\mu^2$, and ϕ is the appropriate azimuthal angle measured from the $k-K$ plane. The function $p(\vec{k},\vec{k}')$ stands for $V|\langle k|V_s|k'\rangle|^2/\pi\hbar$. The $A(\vec{k})$ can be expressed in terms of these quantities,

$$ A(k) = v_F \sum_C \{\mu[1-2\beta^2(k)]_0 m_C - {}_{\parallel}m_C\} \,, \tag{3.2} $$

where $v_F = \hbar k_F/m^*$ is the velocity at the undisturbed Fermi surface. It will be convenient to abbreviate the sum of any m_C over the cells by

$$ \sum_C {}_x m_C = {}_x m_t \,. \tag{3.3} $$

To distinguish those effects arising from phonon umklapp, from those due to Bragg coupling Sec. III A gives a treatment using only single wave functions.

A. Single-plane-wave approximation

Under this limitation $\alpha_K = 1$ and $\beta_K = 0$, v becomes proportional to μ, and the distortion of the Fermi surface is neglected.

For the cell I the range of the integration is limited to the part of the Fermi surface enclosed in the cell. With a spherical-cell approximation the integration is simple using $\vec{k}$ as the polar axis. Since the phonon cell and the volume enclosed by the Fermi surface are equal for a divalent metal, the area of integration subtends a solid angle of π at the $\vec{k}$-space origin. With no umklapp the phonon structure factor is unity. The expressions for ${}_0m_I$, ${}_{\parallel}m_I/\mu$, and ${}_{\perp}m_I/\nu$,

$$ \frac{{}_0m_I}{m_0} = \frac{1}{2}\int_{1/2}^{1}\left(\frac{F(q)}{F(0)}\right)^2 d\mu = \frac{1}{4}\left(1-\frac{1}{2b}+\frac{1}{12b^2}\right) \,, \tag{3.4a} $$

$$ \frac{{}_{\parallel}m_I}{m_0} = \frac{\mu}{2}\int_{1/2}^{1}\left(\frac{F(q)}{F(0)}\right)^2 \mu'\,d\mu' = \frac{\mu}{4}\left(\frac{3}{4}-\frac{1}{3b}+\frac{5}{96b^2}\right), \tag{3.4b} $$

$$ {}_{\perp}m_I/\nu = {}_{\parallel}m_I/\mu \,, \tag{3.4c} $$

are independent of angular coordinates. They are here expressed in dimensionless form, where the constant m_0 is

$$ m_0 = (2\pi m^* k_F/h^3)\,F_0^2(kT/\rho C_l^2) \,. \tag{3.5} $$

(Here $\rho = MN/V$ is the metal density.) Further, the contribution to $A(\vec{k})$ from this cell can also be written

$$ \mu\,{}_0m_I - {}_{\parallel}m_I = \frac{\mu}{4}\left(\frac{1}{4}-\frac{1}{6b}+\frac{1}{32b^2}\right)m_0 \,. \tag{3.6} $$

When k' lies in cell II umklapp is involved by a vector $\vec{Q} = -2k_F\gamma$ along a coordinate axis. Again we use the spherical-phonon-cell approximation. The advantages are that practically every expression can be integrated in closed form and that in studying transport behavior as a function of T below the Debye temperature, the cell radius can be directly related to the largest available phonon wave number. The geometry is shown in Fig. 3. By inspection one can deduce the following nomenclature and relations. The length of the vector $\vec{k}+\vec{Q}$ is ek_F, where we have

$$ |e| = (1-4\mu\gamma+4\gamma^2)^{1/2} \,. \tag{3.7} $$

The angle that $\vec{e}$ makes with the Z axis is $\pi-\xi$;

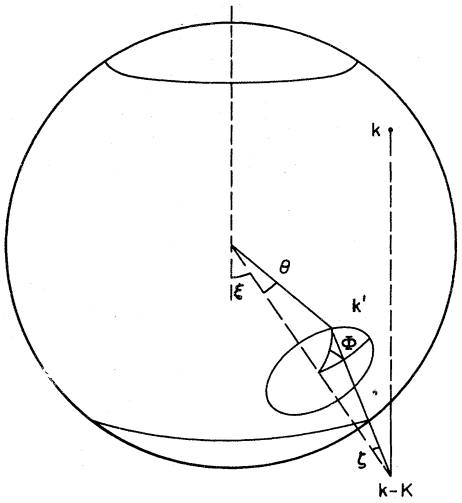

FIG. 3. Geometry for cell-II scattering with spherical phonon zone.

$\cos\xi = (2\gamma - \mu)/e$ and $\sin\xi = \nu/e$.

The line of centers can be used as a polar axis and the angles θ and Φ are the spherical polar angles which map out the position of $\vec{k}'$, the variable of surface integration as seen from the k-space origin. From the end of $\vec{e}k_F$ the analogous angles are ζ and ϕ. The interrelationships are

$$\cos\zeta = (e - \cos\theta)k_F/q \,, \tag{3.8a}$$

$$\sin\zeta = (k_F \sin\theta)/q \,. \tag{3.8b}$$

Of course, $\vec{q}$, the phonon wave-number vector, goes from $\vec{k}'$ to $\vec{e}k_F$. It is related to e by

$$q^2 = (e^2 + 1 - 2e\cos\theta)k_F^2 \,. \tag{3.9}$$

Preparatory to finding the m's we now express the phonon structure factor and $F(k)$ in terms of variables ζ and ϕ. The structure factor of the phonons squared is fundamentally

$$S_p^2 = \frac{kT}{Mc_l^2}\left[\left(1 + \frac{Q\cos\chi}{q}\right)^2 + r^2\left(\frac{Q\sin\chi}{q}\right)^2\right], \tag{3.10}$$

where r is c_l/c_t, the ratio of the velocity of longitudinal acoustic phonons to that of the transverse phonons. The angle χ is between the direction of $\vec{q}$ and $\vec{Q}$; its value is determined by

$$-\cos\chi = \cos\xi\cos\zeta + \sin\xi\sin\zeta\cos\phi \,. \tag{3.11}$$

Here the choice for $\phi = 0$ corresponds to $\vec{k}'$ in the same plane as $\vec{e}$ and $\vec{k}$ and lying between them. The substitution of Eq. (3.11) in (3.10) gives

$$S_p^2 = \frac{kT}{Mc_p^2}\left[1 - \frac{2Q}{q}\cos\xi\cos\zeta + \left(\frac{Q}{q}\right)^2[r^2 + (1-r^2)(\cos^2\xi\cos^2\zeta + \sin^2\xi\sin^2\zeta\cos^2\phi)]\right.$$
$$\left. - \frac{2Q}{q}\sin\xi\sin\zeta\cos\phi\left(1 + (r^2-1)\frac{Q}{q}\cos\xi\cos\zeta\right)\right] \,. \tag{3.12}$$

In a similar way the expression for $F^2(\kappa)$ in Eq. (2.19) can be expanded to

$$F^2 = F_0^2\left[\left(1 - \frac{1}{2bk_F^2}(q^2 - 2Qq\cos\xi\cos\zeta + Q^2)\right)^2 + \frac{2Qq}{k_F^2 b}\sin\xi\sin\zeta\cos\phi\right.$$
$$\left.\times\left(1 - \frac{1}{2bk_F^2}(q^2 - 2Qq\cos\xi\cos\zeta + Q^2)\right) + \left(\frac{Qq}{k_F^2 b}\sin\xi\sin\zeta\cos\phi\right)^2\right]. \tag{3.13}$$

Substitution of these expressions into Eq. (3.1a) by virtue of Eq. (2.13) gives the following expression, after integration over ϕ:

$${}_0m_{II} = \frac{m_0}{2}\int_{e/2}^{1} d(\cos\phi)\left\{\left[1 - \frac{2Q}{q}\cos\xi\cos\zeta + \left(\frac{Q}{q}\right)^2[r^2 + (1-r^2)(\cos^2\xi\cos^2\zeta + \tfrac{1}{2}\sin^2\xi\sin^2\zeta)]\right]\right.$$
$$\times\left(1 - \frac{1}{2bk_F^2}(q^2 - 2qQ\cos\xi\cos\zeta + Q^2)\right)^2 + \frac{1}{2}\left[1 - \frac{2Q}{q}\cos\xi\cos\zeta + \left(\frac{Q}{q}\right)^2[r^2 + (1-r^2)\cos^2\xi\cos^2\zeta]\right]$$
$$\times\left(\frac{Qq}{k_F^2 b}\sin\xi\sin\zeta\right)^2 + \frac{3}{4}\left(\frac{Q^2}{k_F^2 b}\right)^2(1-r^2)\sin^4\xi\sin^4\zeta - \frac{2}{b}\left(\frac{Q}{k_F}\right)^2\sin^2\xi\sin^2\zeta$$
$$\left.\times\left(1 - \frac{1}{2bk_F^2}(q^2 - 2Qq\cos\xi\cos\zeta + Q^2)\right)\left(1 + (r^2-1)\frac{Q}{q}\cos\xi\cos\zeta\right)\right\} \,. \tag{3.14}$$

Somewhat more complicated expressions evolve for ${}_{\parallel}m_{II}$ and ${}_{\perp}m_{II}$. Here one must use the substitutions,

$$\mu' = -\cos\xi\cos\theta + \sin\xi\sin\theta\cos\phi \,, \tag{3.15a}$$

$$\nu' = \sin\xi\cos\theta + \cos\xi\sin\theta\cos\phi \,. \tag{3.15b}$$

Although the integration over $\cos\theta$ can generally be carried out, it proved to be a reasonable ap-

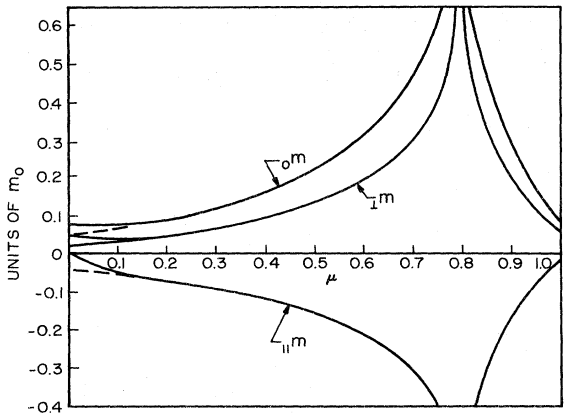

FIG. 4. Plot of $_0m_{II}$, $_\parallel m_{II}$, and $_\perp m_{II}$ for single-plane-wave approximation with spherical phonon cell.

proximation to replace $\cos\theta$ where it appears in the numerator by its average value, $\frac{1}{2}+\frac{1}{4}e$. The leading term in S_p^2 is $(rQ/q)^2$ and its integral gives rise to a logarithmic singularity as $\theta \to 0$ for $\mu=\gamma$, where q^2 becomes $1-\cos\theta$. This is, of course, the cause of the "hot spot" situation mentioned earlier.

It is not easy to get much additional feeling for the general behavior of the m's without resorting to numerical evaluation. This we did, cross checking direct computer integration of equations such as (3.14) with evaluation of the expressions resulting from analytic integration. We needed constant values to assign to the constants γ, r, b, and g. For γ we chose 0.80, very close to the value that one would find for a perfect Fermi sphere of a divalent metal in a simple cubic lattice. For r we chose $(2)^{1/2}$—certainly a reasonable choice. For b the latitude for selection was wider, but it seemed clear that a great number of pseudopotentials give form factors with zeros less than $2k_F$. We picked a value for b of 1.80 which gave a crossing at $k=1.9k_F$. This choice fixed the value of g (near $T=0$) at 0.12 although a lower value could have been equally reasonable in view of the high-temperature applications in view. The ensuing plots for $_0m_{II}$, $_\parallel m_{II}$, and $_\perp m_{II}$ are shown in Fig. 4. One notes that all three have relatively small values in the equatorial region (low μ), increase to a logarithmic singularity at the zone plane, and in the cap region ($|\mu|>\gamma$) appear somewhat smaller, falling rather rapidly on approaching the pole ($\mu=1$).

The $_0m$ is naturally the largest, $_\perp m$ appears to scale rather closely with $_0m$, and $_\parallel m$ is negative, since cell II is mainly in the lower hemisphere. From symmetry $_\parallel m$ must vanish at the equator as indicated by the solid line. The dotted line shows the contribution from the lower hemisphere only. One must include also k' in the upper cap region as part of cell II when k is close to the equator. As a result the value of $_\parallel m$ goes to zero at $\mu=0$, its slope is doubled, and there is a slope discontinuity back at $\mu=0.14$, which reflects the point at which the dotted line meets the axis.

We are aware of the limited value of displaying results for a particular choice of material constants. In Sec. III D we shall attempt some general comments on how results may be expected to vary with changes in γ, r, b, and g.

B. Two-plane-wave Bloch functions

With the introduction of electron coupling through the lattice-translational vectors K, the expression for the scattering matrix squared becomes more complex. In place of Eq. (2.13), we have

$$|\langle k|V_s|k'\rangle|^2=(2N)^{-1}\sum_\sigma |a_{q\sigma}|^2 \left|\left(\sum_{K,K'}\alpha_K(k)\,\alpha_{K'}(k')[(\vec{k}+\vec{K}'-\vec{K})\cdot\vec{e}\,]F(\vec{k}+\vec{K}'-\vec{K})\right)\right|^2 . \tag{3.16}$$

For two-plane-wave functions the summations over K and K' include only two values, 0 and minus the K value corresponding to the closest Brillouin zone. (For the equatorial region symmetry may require a three-plane-wave function since there will be two BZ's about equally distant from k.) In terms of the quantities in Eq. (2.15), $\alpha_0=\alpha$ and $\alpha_{-K}=\beta$. The equation for momentum conservation is now $\vec{q}+\vec{Q}$ for the phonons equal to $\vec{k}+\vec{K}'-\vec{K}$. Since each matrix elements will consist of four terms, there will be 16 in all in Eq. (3.16), of which ten are individually different, as compared to what might have been considered a single term for the one-plane-wave function treatment Sec. III A.

Because of the direct μ dependence of the α's and β's the spherical phonon cells offer no advantage at this stage. Accordingly, a cylindrical cell is employed where the cylinder axis is parallel to the relevant $\vec{K}$, and its length is equal to the edge of the cube cell. The geometry is shown in Fig. 5. The mutual consistency of the two treatments is illustrated by Fig. 6, which shows the $_0m$ and $_\parallel m$ (one-plane-wave approximation) for both sphere and cylinder as a function of μ parallel to the cylinder axis. The natural coordinates for the integration over the k' solid angle are μ' and ϕ, where ϕ is now the azimuthal angle re-

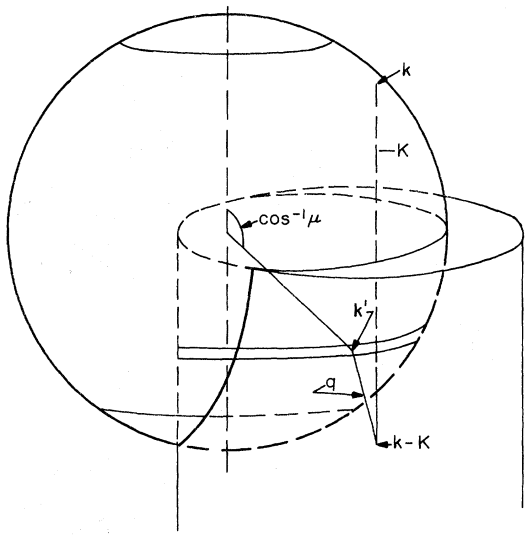

FIG. 5. Geometry for calculation with cylindrical phonon cell.

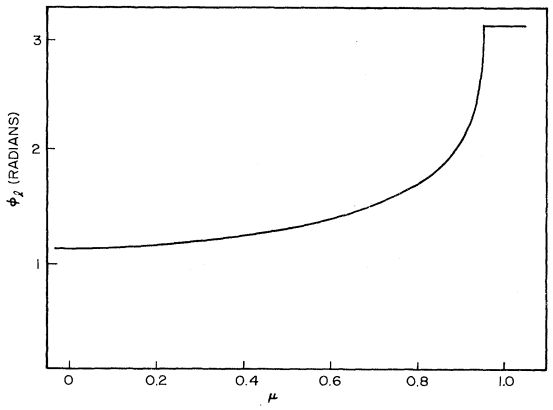

FIG. 7. Illustrative plot of ϕ_i in radians as a function of μ for $\mu=\gamma$.

ferred to the *cylinder* axis. Again the integrations over ϕ can all be carried out in closed form, but the integrations over μ' must be done numerically. The integration limits on ϕ ($\pm\phi_i$) depend on μ' in a complex way; see Fig. 7 where ϕ_i is plotted versus μ' for $\mu=\gamma$. Those terms which contain a q^{-2} require that the deformation of the Fermi surface in the neighborhood of the BZ be taken into account, but the effect is not so serious for other terms, particularly if either $\vec{k}$ or $\vec{k}'$ is far from the BZ.

For the calculation of the m's there are several ways the terms could be combined. We chose to group terms according to the power of the lattice vector (Q or K or combination thereof) appearing in S_ρ. The groups are thereby labeled 0, 1, or 2 and the corresponding parts of the m's will be indexed by a following superscript in parentheses. For terms containing $\vec{q}\cdot\vec{q}$ one has

$$ {}_0m_{\mathrm{I}}^{(0)} = \frac{m_0}{F_0^2}\int_{\mathrm{I}}\frac{d\Omega'}{4\pi}\left[(\alpha\alpha'+\beta\beta')F(q) + \alpha\beta' F(\vec{q}+\vec{Q}) + \alpha'\beta F(\vec{q}-\vec{Q})\right]^2 , \quad (3.17a) $$

$$ {}_0m_{\mathrm{II}}^{(0)} = \frac{m_0}{F_0^2}\int_{\mathrm{II}}\frac{d\Omega'}{4\pi}\left[(\alpha\beta'+\alpha'\beta)F(q) + \alpha\alpha' F(\vec{q}+\vec{Q}) + \beta\beta' F(\vec{q}-\vec{Q})\right]^2 , \quad (3.17b) $$

where the roles of α' and β' are interchanged on going from cell I to II. For the use of the cylindrical coordinates the form factors are written in cell I as

$$ \frac{F(q)}{F_0} = 1 - b^{-1}(1-\mu\mu'-\nu\nu'\cos\phi) = 1 - b^{-1}\frac{1-q^2}{2k_F^2} , \quad (3.18a) $$

$$ \frac{F(q\pm Q)}{F_0} = 1 - b^{-1}\left(\frac{q^2}{2k_F^2} \pm 2\gamma(\mu'-\mu) + 2\gamma^2\right); \quad (3.18b) $$

and in cell II, where μ' is for the most part negative, we have

$$ \frac{F(q)}{F_0} = 1 - b^{-1}[1+\mu\mu' - 2(\mu-\gamma)(\mu'+\gamma) - \nu\nu'\cos\phi] , \quad (3.19a) $$

$$ \frac{F(q\pm Q)}{F_0} = 1 - b^{-1}\left(\frac{q^2}{2k_F^2} + 2\gamma(\mu-\mu')(1\pm1) + 2\gamma^2(1\pm1)\right) . \quad (3.19b) $$

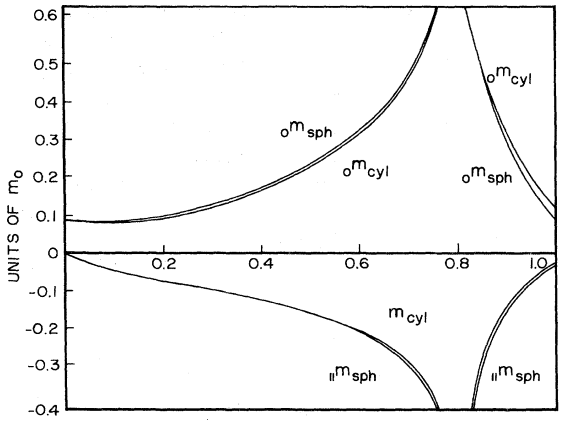

FIG. 6. Comparison of $_0m$ and $_{II}m$ for cylindrical vs spherical cells as a function of μ.

In the succeeding plots of the various functions that were numerically determined as functions of κ the introduction of the distortion of the Fermi surface made it necessary to distinguish between the definition of μ as the projection of $\vec{k}$ in units of k_F or as the cosine of the angle which $\vec{k}$ makes with the Z axis. It was decided that the former is

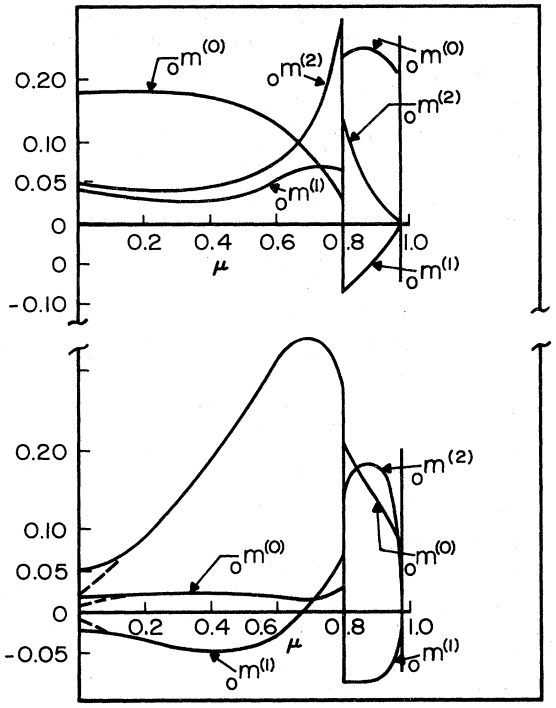

FIG. 8. Plots of ${}_0m_{\rm I}$ and ${}_0m_{\rm II}$ as functions of μ: (a) ${}_0m_{\rm I}^{(0)}$, ${}_0m_{\rm I}^{(1)}$, and ${}_0m_{\rm I}^{(2)}$; (b) ${}_0m_{\rm II}^{(0)}$, ${}_0m_{\rm II}^{(1)}$, and ${}_0m_{\rm II}^{(2)}$.

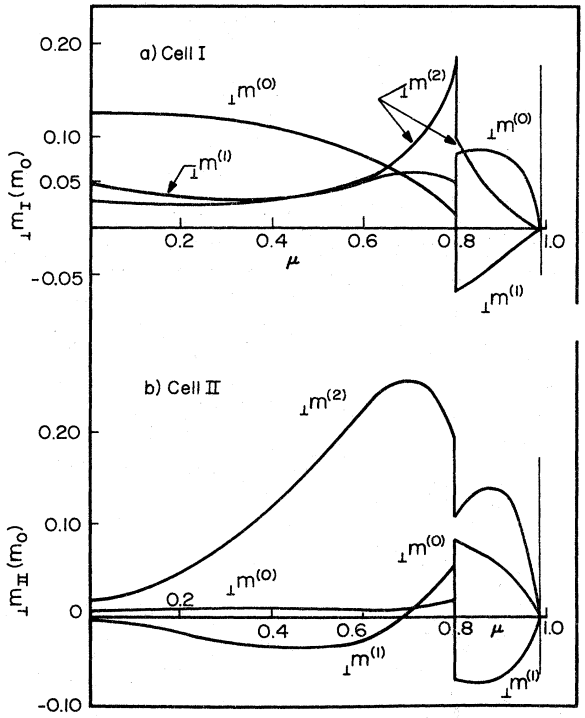

FIG. 10. Plots of $m_{\rm I}$ and $m_{\rm II}$ as functions of μ: (a) ${}_\perp m_{\rm I}^{(0)}$, ${}_\perp m_{\rm I}^{(1)}$, and ${}_\perp m_{\rm I}^{(2)}$; (b) ${}_\perp m_{\rm II}^{(0)}$, ${}_\perp m_{\rm II}^{(1)}$, and ${}_\perp m_{\rm II}^{(2)}$.

the more useful, since the projection is the natural variable for surface integration when there is symmetry about an axis. With this choice the dis-

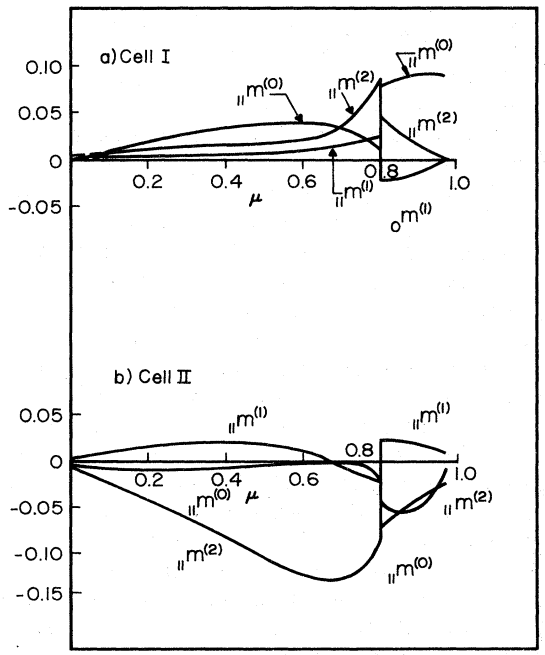

FIG. 9. Plots of ${}_\parallel m_{\rm I}$ and ${}_\parallel m_{\rm II}$ as afunctions of μ: (a) ${}_\parallel m_{\rm I}^{(0)}$, ${}_\parallel m_{\rm I}^{(1)}$, and ${}_\parallel m_{\rm I}^{(2)}$; (b) ${}_\parallel m_{\rm II}^{(0)}$, ${}_\parallel m_{\rm II}^{(1)}$, ${}_\parallel m_{\rm II}^{(2)}$.

continuity at the zone occurs at $\mu=\gamma$ without a break in the abscissa and the point with polar symmetry is indicated by a value of μ somewhat less than 1.

Plots of ${}_0m_c^{(0)}$ vs μ are shown in Figs. 8(a) and 8(b). The substantial contribution from cell I at low μ is in large part from the free-electron term. The discontinuities at $\mu=\gamma$ arise from the several $\alpha\beta$ terms that develop on squaring Eqs. (3.17a) and (3.17b). The particular interest in this (0) group comes from the fact that the phonon structure factor does not appear (S_p is constant). With a change of the appropriate multiplicative constant these results then cover the case of impurity scattering to all powers of β. This was the problem treated by Feit and Huntington,[17] who solved the Boltzmann equation self-consistently but to only first order in the perturbation parameter.

The plots for ${}_\parallel m_c^{(0)}$ and ${}_\perp m_c^{(0)}$ are shown in Figs. 9 and 10, respectively. The relative smaller size here of ${}_\parallel m_c$, compared to the situation in Fig. 4, comes from the factor $1-2\beta^2$ in Eq. (2.16) which did not appear in Sec. IIIA.

Proceeding on to group (1) we deal with the cross terms in S_p involving $\vec{q}\cdot\vec{Q}$,

$$
\begin{aligned}
{}_0m_{\rm I}^{(1)} = m_0 F_0^{-2} \int_{\rm I} \frac{d\Omega'}{4\pi} \frac{2\vec{q}\cdot\vec{Q}}{q^2} &[(\alpha\alpha'+\beta\beta')F(q) \\
&+ \alpha\beta'(q+Q)+\alpha'\beta F(q-Q)] \\
&\times[\alpha\beta' F(q+Q) - \alpha'\beta F(q-Q)]\,, \qquad (3.20a)
\end{aligned}
$$

$$ {}_0m_{II}^{(1)} = m_0 F_0^{-2} \int_{II} \frac{d\Omega'}{4\pi} \frac{\vec{q}\cdot\vec{Q}}{q^2} [(\alpha\beta' + \alpha'\beta)F(q) + \alpha\alpha' F(q+Q) + \beta\beta' F(q-Q)] \times [\alpha\alpha' F(q+Q) - \beta\beta' F(q-Q)] . \quad (3.20b) $$

The plots of these functions also appear in Figs. 8–10. One notes that these functions are small, particularly at low μ, the result of considerable internal cancellation. There is, however, a good size discontinuity at $\mu = \gamma$ which tends to cancel in large measure the discontinuities in the $m_C^{(0)}$.

Many of the integrations over ϕ at this stage involve q^{-2} where the common geometry in such integrations includes the arc of a circle ($-\phi_I < \phi < \phi_I$) and a symmetrically placed point P. Then q is the variable distance from P to any point on the circular arc. Unless P lies in the plane of the circle, the circle and P determine a sphere on whose surface they lie. (This sphere will be the Fermi sphere only in cell I when distortion is neglected.) Figure 11 shows the geometry. From a knowledge of the Fermi-surface distortion and the μ's one can determine the radius ν of the arc, the distance y of P from the plane of the arc, and the distance x of P from the axis. In these terms the radius of the sphere is

$$ R = \{\nu^2 + [(x^2 + y^2 - \nu)^2/2y]^2\}^{1/2} . $$

With the use of this construction and a standard integration formula[18] the integral becomes

$$ \int_{\phi_I}^{\phi_I} q^{-2}\, d\phi = \frac{2}{yR} \tan^{-1}\left(\frac{\frac{1}{2} yR \tan\phi_1}{d^2}\right) , \quad (3.21) $$

where d^2 is the square of the distance from P to the center of the arc (nearest point), or $y^2 + (\nu - x)^2$. If $\frac{1}{2}\pi < \phi_I < \pi$, the integral can be roughly approximated by π/yR. The remaining integrations over μ' are then simple.

The plots for ${}_{\parallel}m_C^{(1)}$ and ${}_{\perp}m_C^{(1)}$ are shown in Figs. 9 and 10, respectively. The terms which involve

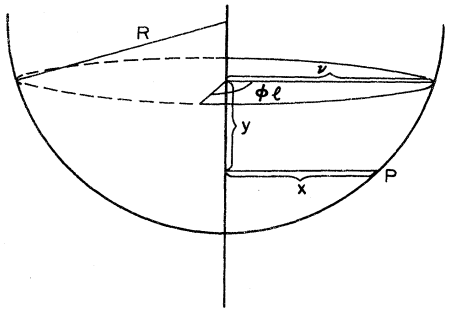

FIG. 11. Construction for integration of q^{-2} terms.

$\vec{Q}\cdot\vec{Q}$ compose group (2). These are the ones which give rise to the logarithmic singularities for the single-plane-wave approximation in Sec. III A. Here no singularity develops. It has been pointed out in the literature[19] that this is the result of a zero in the matrix element [Eq. (3.16)], but this is only part of the reason. The equations for ${}_0m_C^{(2)}$ are given below,

$$ {}_0m_I^{(2)} = m_0 F_0^{-2} \int_I \frac{d\Omega'}{4\pi} \left(\frac{Q}{q}\right)^2 [r^2 - (r^2-1)\cos^2\chi] \times [\alpha\beta' F(\vec{q}+\vec{Q}) - \alpha'\beta F(\vec{q}-\vec{Q})]^2 , \quad (3.22a) $$

$$ {}_0m_{II}^{(2)} = m_0 F_0^{-2} \int_{II} \frac{d\Omega'}{4\pi} \left(\frac{Q}{q}\right)^2 [r^2 - (r^2-1)\cos^2\chi] \times [\alpha\alpha' F(\vec{q}+\vec{Q}) - \beta\beta' F(\vec{q}-\vec{Q})]^2 . \quad (3.22b) $$

The condition that formerly gave rise to a singularity was for μ' and μ both to approach γ, and for ϕ to go to 0. This means $q \to 0$. The magnitudes of α, α', β, and β' all approach $\frac{1}{2}$ but the sign of β and β' will be the same only if $\vec{k}$ and $\vec{k}'$ belong to the same band, i.e., $|\mu|$ and $|\mu'|$ are both greater or both less than γ. If so, then the last terms in square brackets in both of the Eqs. (3.22) will vanish at the former point of singularity. If $\vec{k}$ and $\vec{k}'$ are not in the same band, then the last terms in square brackets do not vanish but neither does $\vec{q} \to 0$, because of the distortion of the Fermi surface—so again no singularity, although this situation does not appear to have been particularly noted before.

The shapes for the curves of ${}_0m_C^{(2)}$, ${}_{\parallel}m_C^{(2)}$, and ${}_{\perp}m_C^{(2)}$ appear in Figs. 8–10, respectively. In all cases there is a large discontinuity at the zone so that the m's are smaller in absolute value in the polar region. Discontinuities for transport parameters at the zone have been well studied,[20] particularly for impurity scattering, and we have seen them also with the (0) and (1) terms. This situation is, however, somewhat different in that the sign of the discontinuity does not depend on the sign of the matrix element associated with the zone gap.

It remains now to combine the results of Figs. 8–10 to get ${}_0m_C$, ${}_{\parallel}m_C$, and ${}_{\perp}m_C$ as shown in Figs. 12(a)–12(c), respectively. These plots emphasize that ${}_0m$ and ${}_{\perp}m$ have the same values but equal slopes of opposite sign for cells I and II at the zone, while the contributions to ${}_{\parallel}m$ from cells I and II are equal in magnitude and opposite in sign. Figure 13 shows the symmetry of the Fermi surface about the zone plane which is the cause of these relations.[5] Because of this symmetry total ${}_{\parallel}m$ vanishes at the zone. This zero matches the zero of $v_{\parallel}$ on the left-hand side of the Boltzmann equation and suggests that one replace Eq. (2.8) by

$$ \tau_1(\vec{k}) = v_F/B(\vec{k}) , \quad (2.8') $$

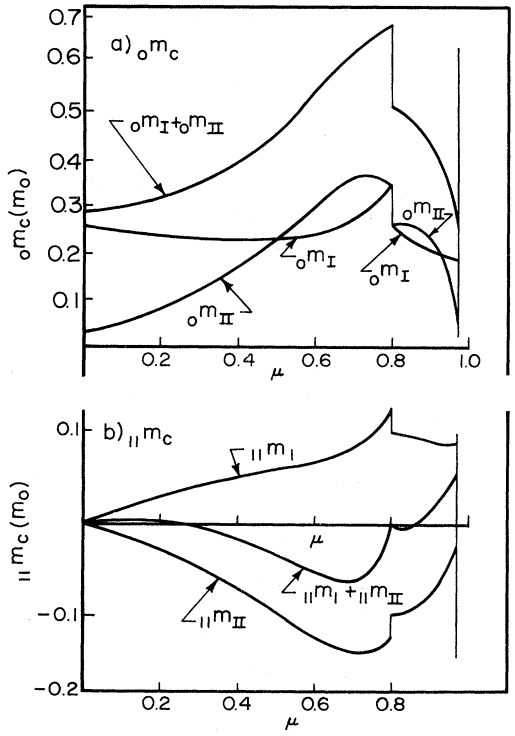

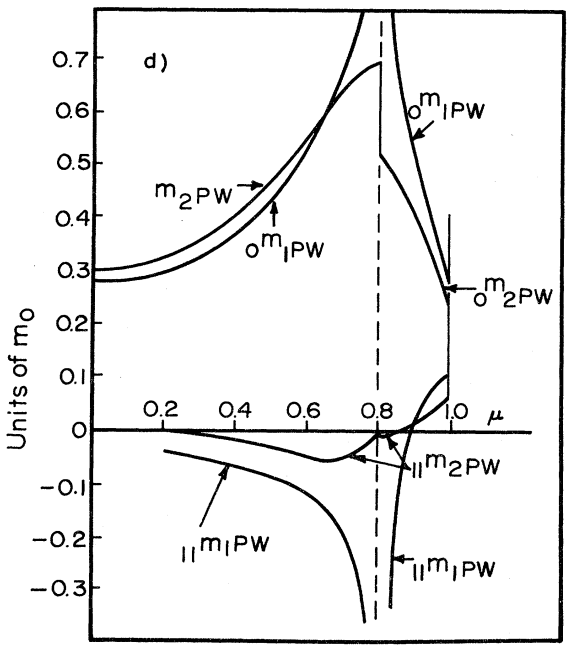

FIG. 12. Plots of the complete m_c as functions of μ: (a) $_0m_I$ and $_0m_{II}$ separately and summed; (b) $_{||}m_I$ and $_{||}m_{II}$ separately and summed; (c) $_\perp m_I$ and $_\perp m_{II}$ separately and summed; and (d) $_0m_I+{}_0m_{II}$ from (a) and an analogous sum from the one-plane-wave calculation. Similar comparison for $_{||}m$.

where the quantity $B(\vec{k})$, defined by

$$B(\vec{k}) = \frac{A(\vec{k})}{\mu[1-2\beta_K^2(k)]} = v_F \sum_c \left({}_0m_c - \frac{{}_{||}m_c}{\mu(1-2\beta_c^2)} \right), \tag{2.8''}$$

has neither a zero or a singularity at the zone.

What has been done so far suffices to give the part of B arising from cells I and IIA, which we shall call B_v, where the subscript v denotes the vertical part. Cell I lies above cell IIA, so that $m_v = m_I + m_{IIA}$. Figure 14 shows the respective contributions of the two parts of B_v in Eq. (2.8''). The horizontal line shows the analogous quantity from the same form factor without umklapp or Bragg scattering, i.e., a free-electron metal with a structureless phonon space. The importance of umklapp in augmenting the scattering is very apparent. These cells I and IIA contribute the main

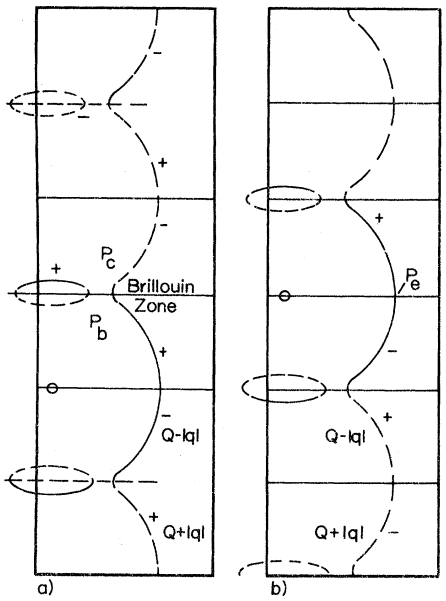

FIG. 13. Symmetry of the extended Fermi surface at the zone plane.

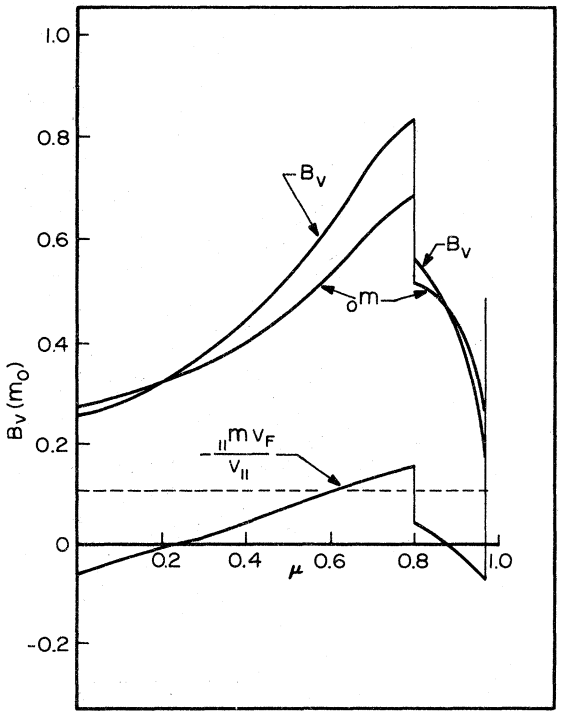

FIG. 14. Combination of $_0m$ and $_{\|}m_I/v_{\|}$.

part of the phonon scattering. Before considering the effect of the rest of the surface in Sec. IV, we shall attempt to use analysis to get more insight into what has been obtained numerically.

C. Analysis of cells I-II scattering

No general analytic approach appeared to be useful over the whole range of μ. Instead, we propose to break the range into three regions and use different approximations in each.

1. Equatorial region

For $\vec{k}$ in the equatorial region it is reasonable to take $\alpha=1$ and $\beta=0$. The quantities appearing in Eq. (3.16) within the large parentheses squared then become for cell I

$$[\alpha'\vec{q}\,F(\vec{q})+\beta'(\vec{Q}+\vec{q})F(\vec{q}+\vec{Q})]^2\,, \tag{3.23a}$$

and for cell II

$$[\alpha'(\vec{q}+\vec{Q})F(\vec{q}+\vec{Q})+\beta'\vec{q}\,F(\vec{q})]^2\,. \tag{3.23b}$$

The principal contributions can be identified as arising from the $(\alpha')^2$ terms for both cells. Except for the factor $(\alpha')^2$ they are the same terms that appear in the single-plane-wave treament previously discussed. For this region α' departs appreciably from unity only for k' near the zone or q_z near $-\frac{1}{2}Q$. For this part of the range of integration, however, the other squared terms with $(\beta')^2$ have approximately the same argument and can be combined with the first terms, effectively supplementing the deficit of $(\alpha')^2$ from unity. There remains then only the term

$$2\alpha'\beta'\vec{q}(\vec{Q}+\vec{q})F(q)F(\vec{q}+\vec{Q}) \tag{3.24}$$

in the integrand for both cells. The β' factor causes considerable cancellation, the ultimate sign being determined by the sign of β' in the $\gamma>|\mu'|$ region. Because this term is small there is a close agreement between the $_0m$ as calculated by the one-plane-wave and two-plane-wave approximations for this region of small μ, as shown in Fig. 12(d), which compares the results for $_0m$ and $_{\|}m$ in these two approximations. This figure also shows a marked decrease for $_{\|}m$ in the low-μ region with the introductions of the second plane wave.

2. Zone region

To explore the zone region we put μ near γ. The m's have maxima here and also marked discontinuities at the zone itself. The appropriate geometry is illustrated in Fig. 13(a) for k at the zone. The point P_c represents k when in the body region. From the symmetry apparent for $|\mu|=\gamma$, cell II is the mirror image of cell I in the reduced scheme of Fig. 13(a). It will be useful to combine together the symmetrically placed states for which the magnitudes of q are the same, but the components parallel to $\vec{Q}$ ($q_{\|}$) are equal and oppositely directed. On this basis the integrals for cells I and II can be coalesced (exactly only for $\vec{k}$ on the zone) and the integrations limited to $q_{\|}>0$. For example, the integrands in Eqs. (3.22) can be combined to give (omitting the part containing $\cos^2\chi$)

$$(rQ/q)^2[(\beta')^2F^2(\vec{q}+\vec{Q})-4\alpha\beta\alpha'\beta'F(\vec{q}+\vec{Q})F(\vec{q}-\vec{Q}) + (\alpha')^2F^2(\vec{q}-\vec{Q})]\,, \tag{2.25}$$

which contributes the dominant term in this region.

As can be seen from Fig. 8, the $_0m^{(2)}$ has a down-drop discontinuity at the zone as does $_0m$ (Fig. 14). From the form of Fq. (3.25) it is clear that a change of sign of $F(\frac{1}{2}Q)$ which changes the sign of β everywhere would not alter the sign of the discontinuity in $_0m^{(2)}$. In the work on zinc,[16] we were surprised to find that under some conditions a change of sign for β can indeed reverse the sign of the discontinuities of the overall m's at the zone. Investigation showed that the $m^{(0)}$ and $m^{(1)}$, although relatively smaller at the zone, varied sensitively in a very complicated way with other parameters, particularly those terms which changed sign with β. In this respect, phonon scattering differs from impurity scattering, where the discontinuities in the scattering integrals at the zone are very simply related to the sign of β.[17,20]

The oversimplified form chosen for $F(q)$ in Eq.

(2.19) gives too large magnitudes for the largest values of the argument used, which are around $2.4k_F$. At one time we were concerned that this unphysical feature of the model might be giving too large a value to Eq. (3.25), and hence too big a discontinuity. A rough calculation showed, however, that an appropriate modification of F in the large-argument region would reduce the contribution of this term and the discontinuity by only about 20%. The primary reason why this defect in $F(q)$ is not more serious is because $F(\vec{q}+\vec{Q})$, which involves the large argument, is always coupled with β', which falls off in this region.

Inspection of Figs. 10 and 12 shows that the ${}_1m$ behavior is generally describable as a scaled down version of the ${}_0m$'s, the reduction being somewhat larger at large μ. For the ${}_{\|}m$'s one again sees the dominant contribution in group (2). The corresponding integrand for $({}_{\|}m_{\mathrm{I}}^{(2)}+{}_{\|}m_{\mathrm{II}}^{(2)})/v_{\|}$ is seen from Eq. (3.22a) to be proportional to

$$\frac{1}{2}\frac{rQ}{q}^2\Big(\left[(\beta')^2F^2(\vec{q}+\vec{Q})-(\alpha')^2F^2(\vec{q}-\vec{Q})\right]-\frac{q}{\alpha^2-\beta^2}\frac{d}{dq}\left[(\beta')F^2(\vec{q}+\vec{Q})\right.$$

$$\left.-2\alpha'\beta'F(\vec{q}+\vec{Q})F(\vec{q}-\vec{Q})+(\alpha')^2F^2(\vec{q}-\vec{Q})\right]_{\substack{z=0\\ \alpha,\beta}}\Big)\left[(\alpha)^2-(\beta)^2\right]\frac{|\mu'|}{\gamma}\ , \tag{3.26}$$

where we have again neglected the term with $\cos^2\chi$ and have used L'Hospital's rule since both the numerator and denominator vanish for $\mu=\gamma$. The second term inside the large parentheses represents the lack of complete cancellation in the integrals, and α and β are here treated as constants when $q\neq 0$ breaks the symmetry. The sign and magnitude of the discontinuity in the quantity (3.26) has been discussed in some detail elsewhere.[21]

Of more interest here is the relative size of ${}_{\|}m/v_{\|}$ to ${}_0m$; which in this application is generally small. The ratio at the zone is about 1 : 7.5 according to Fig. 14 and can be taken as typical. To gain some understanding of this quantity we compare Eqs. (3.25) and (3.26) which present the principal (2) terms in the integrands for the scattering integrals, ${}_0m$ and $-{}_{\|}m/v_{\|}$, respectively. As in the case for the equator ($\mu=0$), one can roughly combine the first and last terms in Eq. (3.25) to obtain $F^2(\vec{q}-\vec{Q})$. The integration over ϕ brings q^{-2} to q^{-1}. The quantity $-4\alpha\beta\alpha'\beta'F(\vec{q}+\vec{Q})\times F(\vec{q}-\vec{Q})$ can be written $\pm g(g^2+q_{\|}^2)^{-1/2}F(\vec{q}+\vec{Q})\times F(\vec{q}-\vec{Q})$, where the minus sign applies for $\vec{k}$ and $\vec{k}'$ on the same surface. On this basis we have for ${}_0m$,

$${}_0m\sim(rQ)^2\int\left(F^2(\vec{q}-\vec{Q})\pm\frac{q}{(g^2+q^2)^{1/2}}\times F(\vec{q}+\vec{Q})F(\vec{q}-\vec{Q})\right)q_{\|}^{-1}\,d\mu'\ . \tag{3.25'}$$

From Eq. (3.26) one sees that the corresponding integrand for ${}_{\|}m/v_{\|}$ contains in its first term the same quantities as appear for ${}_0m$ in Eq. (3.25') with the additional factors $[(\alpha')^2-(\beta')^2]^2\mu/\gamma$. [The second term in Eq. (3.26) contributes primarily to the discontinuity.] These factors reduce the integrand to zero at the equator, give a "narrow" double zero at the zone, and account for the smaller value of ${}_{\|}m/v_{\|}$ compared to ${}_0m$. Because $F(\vec{q}-\vec{Q})$ is large at the equator and decreases as q decreases, the zero at the equator causes the major reduction and one which is largely independent of the material parameters. However, the integrand for ${}_0m$ also increases again near the zone because of the q^{-1} factor. This is more important for the part of the integration where $\vec{k}$ and $\vec{k}'$ are on different parts of the reduced surface when the sign for the second term in Eq. (3.25') is positive. Consequently, the effect of the double zero at the zone can also be important. This effect increases with g, the electron-lattice coupling parameter. Since g is large in the example we have chosen, one might expect the ratio of ${}_0m$ to ${}_{\|}m/v_{\|}$ may, in general, be somewhat smaller than found here. Far removed from the zone, however, ${}_{\|}m/v_{\|}$ can indeed become quite large. We have found[16] in the case of large r and small g the cancellation between cells I and IIA is by no means as complete as in the example chosen here.

3. *Cap region*

The principal feature of the scattering integrals in the cap region is the rapid decrease which frequently appears as $\mu\to 1$. While many elements enter into the calculations, the only one which varies rapidly in this region is $F(\vec{q}+\vec{Q})$, which has an accidental zero for the value of the distance between the pole and the far zone (accidental in view of the particular material parameters chosen). However, much the same sort of behavior should result from other specific form factors of reasonable shape.

More specifically in the case of the cell-I integrals both ${}_0m_{\mathrm{I}}^{(1)}$ [Eq. (3.20a)] and ${}_0m_{\mathrm{I}}^{(2)}$ [Eq. (3.22a)] show factors of $\alpha\beta'F(\vec{q}+\vec{Q})-\alpha'\beta F(\vec{q}-\vec{Q})$. At the pole this quantity has a zero; at the zone, where β' has a cusped maximum, $F(\vec{q}+\vec{Q})$ has the above-mentioned accidental zero; and over the body por-

tion of cell I the two terms are opposite in sign and nearly equal in magnitude. These considerations explain why these quantities are so small at the pole (particularly ${}_0m_{\rm I}^{(2)}$, which contains this factor squared), and why the two-plane-wave approximation lies below the one-plane-wave approximation as shown in Fig. 12(d).

For cell II it is ${}_0m_{\rm II}^{(0)}$ which decreases rapidly in value. A glance at Eq. (3.17b) shows that the $\alpha\alpha'$ terms could be expected to dominate, but again this is the term with $F(\vec{q}+\vec{Q})$, so that its decrease with $\mu \to 1$ is to be expected. The same general considerations apply also to the ${}_{\parallel}m$'s and the ${}_{\perp}m$'s in the cap region as can be seen in Figs. 9 and 11.

D. Parameter variation

What general conclusions can be drawn from the specific numerical solutions as to how the scattering curves might be altered by changes in the material parameters: γ, r, g, and b?

The parameter γ primarily functions to mark the position of the zone with its accompanying maximum and discontinuity. Secondarily, it gives the size of Q and so determines the dimensions of the phonon cells. The influence of this aspect of γ is more difficult to assess.

The ratio r of the longitudinal to transverse velocity of sound affects the relative influence of the umklapp to normal interactions, since transverse phonons are involved only in umklapp, where they tend to dominate the longitudinal phonons. As noted earlier, the low frequencies are particularly effective in the umklapp process. While discussing the phonon spectrum here, it is appropriate to point out that a refinement of the method to include the effect of phonon dispersion would tend to put more weight on the higher phonon modes, since dispersion considerations would lower their frequencies. Conversely, a calculation of phonon scattering at temperatures low enough to be in the region of Θ_D would necessarily eliminate the highest-frequency phonons. Again it is not easy to see how this consideration might alter the shapes of the various m curves.

In subsequent work[16] we have found that increasing the size of r has one interesting effect that had not been anticipated. In cell II, the transverse phonons (which are favored by large r) are dominant in scattering to that region of the Fermi surface for which $\mu' \cong \mu - 2\gamma$. For small μ this region is missing, but the m's increase rapidly as μ increases and show negative curvature in the $0.4 < \mu < 0.5$ region when r is large instead of the uniform upward concave behavior shown in our example here where r is small, i.e., 1.4.

The quantity b plays a crucial role in determining the shape of $F(q)$, since it sets the zero for this function. The approximation of using an $F(q)$ linear in q^2 is clearly unphysical at large arguments. As was pointed out in Sec. III C, this shortcoming turns out to be not too serious for a b as large as 1.8, but for an appreciably smaller b the need for another term in the expansion of F may occur once values of the argument larger than $2k_F$ are introduced by the Bragg coupling. The influence of the b parameter is easiest to assess for those terms where umklapp and Bragg coupling are not involved and closed-form expressions can be obtained, e.g., the free-electron terms (3.3a) and (3.3b), which dominate the $m_{\rm I}$ in the low-μ region. Here a change of b from 1.8 to 1.5 brings a change to all quantities of roughly +10% including the significant combination ${}_0m_{\rm I} - {}_{\parallel}m_{\rm I}/\mu$. Quite a different story results if the integration is extended over the whole surface instead of being confined to cell I. The result so obtained is proportional to an inverse relaxation time in a situation where neither umklapp nor Bragg coupling is operative, and therefore supplies a useful number for over-all comparison (see Sec. VI). One obtains

$$ {}_0m_\Omega - \frac{{}_{\parallel}m_\Omega}{\mu} = \frac{1}{2}\int_{-1}^{1} \frac{F^2(\mu')}{F_0^2}\left(1-\frac{\mu'}{\mu}\right)d\mu' $$

$$ = 1 - \frac{8}{3b} + \frac{2}{b^2} \quad . \tag{3.27} $$

Here the subscript Ω denotes averaging over all solid angles. The final result has a minimum of 0.111 at $b = 1.50$ and for $b = 1.8$ it has the value 0.125.

The quantity g is essentially the expansion parameter of the nearly-free-electron-metal (NFEM) approximation. Its upper value is controlled by $F(k)$, but it may be less owing to temperature (Debye-Waller factor) or other causes for departure from crystalline regularity. Its effect shows predominantly in the zone regions. The magnitudes of the m's in these regions and of their discontinuities are directly proportional to g—except that right at the zone itself all the $m^{(2)}$ have a $-\ln g$ term. As a result really small values of g will generate thin spikes there. In the limit these have negligible effect. Of course, the distortion of the Fermi surface is directly proportional to g.

A good deal of work has been reported on transport properties of polyvalent metals[4,10,11] in the one-plane-wave approximation, essentially $g = 0$, with on the whole quite satisfactory agreement with observed conductivity. We find [see Fig. 12(d)] that the electron coupling makes relatively little difference in the small-μ region and even over most of the cap region the two-plane-wave result is within 80% of the one-plane-wave value in spite of the large value of $\vec{g}$ chosen in this work.

IV. SCATTERING INTEGRALS FOR OTHER CELLS

In the treatment of cells I and IIA in Sec. III, the fact that $\vec{K}$ and $\vec{Q}$ were parallel to the direction of the electric field gave a sort of one-dimensional simplicity. In this section the scattering to other cells is considered. In the spirt of the (NFEM) approximation, one would expect this process might be simply additive. This is indeed the result to first order from a procedure which involves treating two Brillouin zones simultaneously with what amounts to a four-plane-wave approximation. Additional terms do appear, but they are all small enough to be unimportant.

A sample wave function to involve the coupling with K_x and K_z simultaneously might have the following form:

$$\psi_{\vec{k}}(\vec{r}) = (\alpha_x e^{ik_x x} + \beta_x e^{i(k_x - k_x)x}) \times (\alpha_z e^{ik_z z} + \beta_z e^{i(k_z - k_z)z}) e^{ik_y y} \quad (4.1)$$

for the wave function of a state in cell I. Couplings involving other pairs are obtained by suitable interchanges. Leaving aside for the moment all common factors, we represent the matrix element $\langle k|V|k'\rangle$ in semischematic fashion for cell I,

$$\{(\alpha_x \alpha_x' + \beta_x \beta_x')[q_x] + \alpha_x \beta_x'[q_x + Q_x'] + \alpha_x' \beta_x [q_x - Q_x]\} \times \{(\alpha_z \alpha_z' + \beta_z \beta_z')[q_z] + \alpha_z \beta_z'[q_z + Q_z'] + \alpha_z' \beta_z [q_z - Q_z']\} \cdot [q_y] \ . \quad (4.2)$$

Here the [ ] functionals obey the following product relation:

$$[q_x] \cdot [q_y] \cdot [q_z] \equiv \vec{q} F(|q|) \ , \quad (4.3a)$$

$$[q_x + Q_x] \cdot [q_z - Q_z] \cdot [q_y] \equiv (\vec{q} + \vec{Q}_x - \vec{Q}_z) F(|\vec{q} + \vec{Q}_x - \vec{Q}_z|) \ . \quad (4.3b)$$

The indexing system for the phonon cells shown in Fig. 1 is used and extended to cells other than I and IIA. Cells IIB and IIC lie largely in the upper hemisphere and cell IIID includes the area still open in the upper hemisphere. If k' is in cell IIB, the first factor in Eq. (4.2) becomes altered to

$$\{\alpha_x \alpha_x'[q_x + Q_x] + \beta_x \beta_x'[q_x - Q_x'] + (\alpha_x \beta_x' + \alpha_x' \beta_x)[q_x]\} \ . \quad (4.2a)$$

The second z-marked factor would undergo a similar change if k' goes to cell IIIB.

Next, in squaring the matrix elements we have found it useful to keep together the x-marked factors and also the z-marked factors so that

$$|\langle k|V|k'\rangle|_L^2 \sim (A_x + B_x + C_x)(A_z + B_z + C_z)_L \ ,$$

where the L subscript denotes the cell containing $\vec{k}'$. The quantity A_i contains terms with $[q_i]^2$, the C_i contains those terms quadratic in $[q_i \pm Q_i]$, and the B_i contains the cross product terms in $[q_i][q_i \pm Q_i]$. For example, with $L = \mathrm{I}$,

$$(A_i)_{\mathrm{I}} = (\alpha_i \alpha_i' + \beta_i \beta_i')^2 [q_i]^2 \ , \quad (4.4a)$$

$$(B_i)_{\mathrm{I}} = 2(\alpha_i \alpha_i' + \beta_i \beta_i')[q_i] \times \{\alpha_i \beta_i'[q_i + Q_i'] + \alpha_i' \beta_i [q - Q_i]\} \ , \quad (4.4b)$$

$$(C_i)_{\mathrm{I}} = \{\alpha_i \beta_i'[q_i + Q_i'] + \alpha_i' \beta [q_i - Q_i]\}^2 \ . \quad (4.4c)$$

[Of course the evaluation of the complete scattering integrals involves multiplying all terms by $(2\pi/h) \times (k^2 d\Omega / 4\pi \nabla_k \epsilon)(kT/M\omega_0^2)$, summing over polarizations, and integrating over solid angle.]

In organizing the evaluation of these many terms we have chosen to divide them into two groups. The first group, which are the larger and are expressible in terms of quantities studied in Sec. III, have been chosen to be

$$\sum_L [A_x(A_z + B_z + C_z) + A_z(A_x + B_x + C_x) - A_x A_z]_L \ . \quad (4.5a)$$

The group of the remaining terms consists of

$$\sum_L [B_x B_z + B_x C_z + B_z C_x + C_x C_z]_L \ . \quad (4.5b)$$

Each terms in Eqs. (4.5) is the product of two matrix elements and each matrix element is composed of an x and a z part drawn, respectively, from the two quantities designated by capital letters. How this pairing is done is unimportant where the symmetric quantities A_i or C_i are involved. Ambiguity arises only when the $B_x B_z$ product is involved. Here two possible terms evolve, one with $[q + Q_x + Q_z][q]$ and the other with $[q + Q_x][q + Q_z]$.

To return to Eq. (4.5a) let us write $A_i = N_i[q][q]$. Then $A_x(A_z + B_z + C_z)$, which we call the "vertical term," gives just $N_{x0} m(\mu)$. In cells I and IIA, $N_{x\mathrm{I}} = (\alpha_x \alpha_x' + \beta_x \beta_x')^2$, and it is usually close to unity except when k_x is near $\pm \frac{1}{2} K_x$, where N_x dips sharply. In the cells IIB and IIIB, $N_{x\mathrm{II}} = (\alpha_x \beta_x' + \alpha_x' \beta_x)^2$ is much smaller everywhere except near the vertical zone where it peaks sharply. $A_z + B_z + C_z$ is the same at the zone planes in both cells so that one can roughly combine the two contributions together. Again $N_{x\mathrm{I}} + N_{x\mathrm{II}}$ supplement each other and in this region give a sum of $1 \pm 2\langle \alpha_x' \beta_x' \rangle$, which is near unity. The A factor is large in cell I and one other adjacent cell (in this case cell IIA) and negligible elsewhere on the Fermi surface except where it has a cusped maximum, which supplements the cusped minimum mentioned above.

The principle of the development is the same for $A_z(A_x + B_x + C_x)$, which we call the "horizontal term."

Looking at the $A_z A_x$, which must be subtracted in Eq. (3.5a), we see again a quantity which is large and nearly unity in cell I only. Certain cusped minima that occur are again compensated for the average by cusped maxima in other cells,

which otherwise make negligible contributions. As such this term reduces to ${}_0m_{\mathrm{I}}^f$, the scattering integral for one plane wave over cell I, as in Eq. (3.4a). The effect of this term is then simply to prevent the double counting of $A_z A_x$ in cell I.

The many terms in Eq. (4.5b) have been evaluated roughly elsewhere[21] and found to be small for the most part. Attention is concentrated, therefore, on the quantities in Eq. (4.5a).

At this point some perspective is possible of how the four-plane-wave approach can be used to handle simultaneously two sets of Brillouin zones and even to extend to situations of greater complexity. The method should be generally applicable to metals of more complex cell structure than that of the fictitious model metal. In this calculation the general procedure is embodied in the equation

$$ {}_0m_t = \sum_L ({}_0m_{\mathrm{I}}^L + {}_0m_L - {}_0m_{\mathrm{I}}^f) + {}_0m_{\mathrm{I}}^f , \tag{4.6}$$

where ${}_0m_{\mathrm{I}}^L$ includes those terms in the integrations over cell I which arise from the coupling with cell I. In the following paper,[16] the same purpose is accomplished perhaps somewhat more accurately by the procedure

$$ {}_0m_t = \sum_L {}_0m_L + {}_0m_{\mathrm{I}}^f \prod_L \frac{{}_0m_{\mathrm{I}}^L}{{}_0m_{\mathrm{I}}^f} . \tag{4.7}$$

Both are workable procedures for treating the scattering integrals in a multiple-zone situation by a pairwise approximation.

The implementation of the application of Eq. (4.6) to the case of the fictitious model metal is shown in Fig. 15. As in prior figures, all quantities are plotted in units of m_0, and as functions of μ or k_z/k_F. The curve with short dashes (a) is just the contribution to ${}_0m_t$ from cells I and IIA, or the "vertical term" almost as shown in Fig. 14. It is discontinuous only for $\mu = \gamma$. The curve with the long dashes is the so-called "horizontal terms" and is composed of the two (equal) contributions to the summation in Eq. (4.6) from L equal to cells IIB and IIC. Because ${}_0m$ has cubic symmetry, the values for these contributions are directly obtainable by a 90° rotation from the cell-IIA calculation. These results are then transformed back to a coordinate system with polar axis along the Z direction and averaged over constant μ. This averaging over ϕ changes a discontinuity in value at $k_x = \gamma k_F$ to a discontinuity in slope at $k_z = (1-\gamma^2)^{1/2} \times k_F$. The curve with alternate dots and dashes (c) shows the small contributions from the ${}_0m_L$ for L equal to cells IIIB, IIIC, and IIID. (These quantities are called $C_x C_z$ in cells IIIB and IIIC, and $C_x C_y$ in cell IIID, and are roughly evaluated in Ref. 21.) Because $(8)^{1/2}\gamma k_F > 2k_F$, the corresponding zones do not intersect the Fermi surface and the Bragg coupling can be neglected. The solid curve (d) gives ${}_0m_t$, the sum of all contributions.

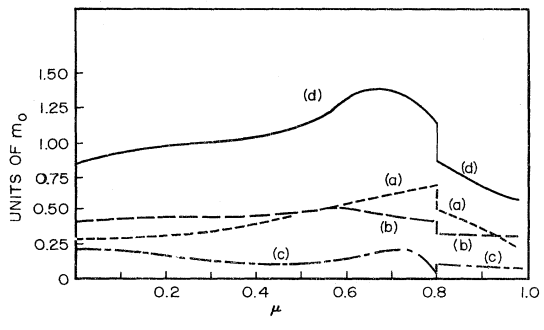

FIG. 15. Contributions to ${}_0m_t$: (a) "Vertical term"; (b) "Horizontal term"; (c) cell-III terms; and (d) ${}_0m_t$.

The treatment of the ${}_{\|}m_t/v_{\|}$ has not been as detailed as that just used for ${}_0m_t$, first because the presence of the additional μ factor in the integrands introduced considerable complications associated with the close cancellations involved, and second because $v_{F\|}m_t/v_{\|}$ is sufficiently smaller for the fictitious model metal than the ${}_0m_t$ to allow a cruder approximation in treating it. That such terms are indeed smaller can be seen from the comparison of ${}_0m$ and $v_{F\|}m/v_{\|}$ in Fig. 14, where the ratio of the first to the second quantity is about 7.5 to 1 for the average values at μ near γ. In Sec. IIIC2, we have shown that the size of this ratio depends only somewhat on the strength of the zone coupling and that it is relatively independent of the other material parameters, so that the ratio will generally be large. (Although the ${}_0m$ happens to be much bigger than ${}_{\|}m/v_{\|}$ throughout the complete range of μ for the fictitious model metal, we have found that this does not necessarily follow in all cases for the low-μ range, particularly when r is large.)

Because the term is small and difficult to evaluate more precisely, we have chosen to estimate it according to the following approximation:

$$\begin{aligned} \frac{v_{F\|}m_t}{v_{\|}} &= \sum_L \int_L p(k,k')v'\,dS'/\,|\nabla_k \epsilon|\,v_{\|} \\ &= \sum_L \int_L p(k,k')\,dS'\langle v'\rangle/\,|\nabla_k \epsilon|\,v_{\|} = \frac{{}_0m_t\langle v'\rangle}{v_{\|}} , \end{aligned} \tag{4.8}$$

where $\langle v'\rangle$ is defined by

$$\langle v'\rangle = \frac{\int_{\mathrm{I'},\mathrm{II'}} p(k,k')v'\,dS'}{\int_{\mathrm{I'},\mathrm{II'}} p(k,k')\,dS'} . \tag{4.9}$$

Here the integrations over cells I′ and II′ are to be taken over the Fermi surface disregarding all but the *horizontal* phonon cell walls and Brillouin zones. With this simplification one can obtain a reasonably satisfactory average for $v_{\|}$ over the

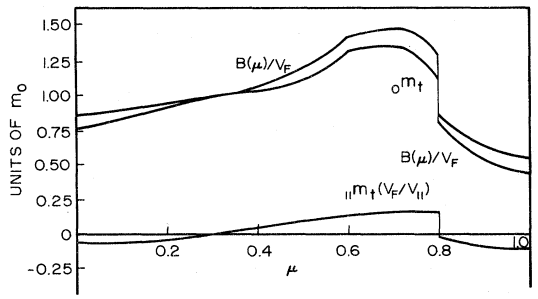

FIG. 16. Plots of $_0m_t$, $_{\|}m_t(v_F/v_{\|})$, and $B(\mu)/v_F$ vs μ.

whole surface. As can be expected, $\langle v'_{\|}\rangle/v_F$ turns out to be small for the fictitious model metal because of extensive cancellation. In Fig. 16, the net $_{\|}m_t v_F/v_{\|}$ is displayed along, with $_0m_t$ from Fig. 15 and their sum which is really the $B(k)$ of Eq. (2.8′). (Note the resemblance to quantities plotted in Fig. 14 for the "vertical" case.) The last quantity, $B(\mu)/v_F$, combines all the scattering integrals which limit the mean free time, since the terms in Eq. (4.5b) are omitted as small. In fact, the $\tau_1(k)$ for the electric field in the z direction is a constant times the reciprocal of B as seen in Eq. (2.8′). It remains only to obtain the subsequent correction to τ_p by iteration.

V. RELAXATION TIME AND ITS APPLICATIONS

The procedure indicated at the end of Sec. IV is now carried out to obtain $\tau_2(k_z)$, the first correction to $\tau_1(k)$. First one inverts $B(\mu)$ to obtain $\tau_1(k_z)$ in units of $(m_0)^{-1}$ as displayed in Fig. 17. Next, one approximates the solution of Eq. (2.11) by replacing $\tau_1(\vec{k}')$ by its average value $\langle\tau_1(k')\rangle$ so that the first square bracket can be brought outside the integral to give

$$\tau_2(k_z) \simeq [\langle\tau_1\rangle - \tau_1(\mu)] \int v(k') W(\vec{k}, \vec{k}')\, d\vec{k}'/A(\vec{k})$$

$$\simeq [\langle\tau_1\rangle - \tau_1(\mu)]\, {}_{\|}m_t(\mu) v_f/A(\vec{k}) \,. \qquad (5.1)$$

The $\tau_1(\mu)$, $\tau_2(\mu)$, and their sum $\tau_p(\mu)$ are also shown in Fig. 17, all in units of $(m_0)^{-1}$. Further iterations are clearly unnecessary.

From a knowledge of τ_p application to numerous transport problems is possible. For example, the conductivity is calculated from the formula

$$\sigma \sim \int_0^1 \tau \hat{E}\cdot\vec{v}\vec{v}\cdot\hat{E}\, dn \,, \qquad (5.2)$$

where $\hat{E}$ is the unit vector in the direction of the electric field (z axis). Numerical integration based on the τ of Fig. 17 and standard variation of $\vec{v}$ gives 0.238 in v_F^2/m_0 for the right-hand side of Eq. (5.2). If this same quantity had been calculated with a constant τ, say, $\langle\tau_1\rangle = 1.26\ (m_0)^{-1}$, the result would have turned out to be 0.208 in v_F^2/m_0. The importance of the variation of τ with position on the Fermi surface becomes more marked when dealing with transport properties which depend sensitively on position with respect to the Brillouin zone, such as Hall coefficient, thermoelectric power, and the wind force in electromigration drive.

VI. CONCLUSIONS

In summary this paper has dealt with the transport problem in a somewhat more direct approach than is currently customary. Most of the recent papers in this area proceed by using the variational technique to calculate upper limits to the resistivity by varying a functional, which embodies effectively the relaxation time. Satisfactory results for the resistivity do not require complete knowledge of the relaxation-time behavior. The method used here proceeds to develop the relaxation time directly from the Boltzmann equation for single-phonon scattering in the high-temperature limit for a model divalent metal. The effects of both umklapp and Bragg scattering have been included. The latter means working in the two-plane-wave approximation and considering also distortions of the Fermi surface. The phonon spectrum has been simplified by omitting anisotropy and dispersion. Although the method is somewhat laborious, we feel it offers two advantages. It affords some direct insight as to how the phonon and electron parameters affect the metal transport and it presents directly the details of the relaxation-time dependence on $\vec{k}$ for a situation where this concept is valid.

In reviewing this calculation, we consider first those results of some generality, next those which seem to be more specific, depending on the parameter values chosen. In this first category is the behavior of the scattering integrals at the Brillouin zone. Not only do they stay finite in the two-plane-wave approximation—for different reasons in the two cases of k and k' on the same or opposite side of the zone—but also what we have

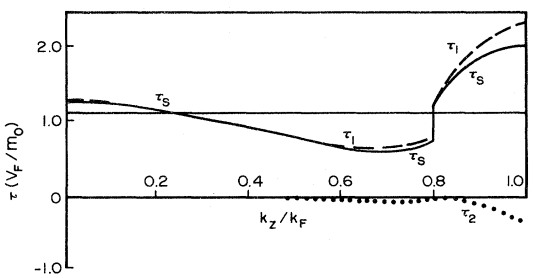

FIG. 17. Plots of $\tau_1(\mu)$, τ_2, and their sum τ_s.

called $_{\|}m$ goes to 0 at the zone from symmetry so that $_{\|}m/v_{\|}$ stays finite also in this region. As a result the relaxation time stays finite, but does exhibit a discontinuity at the zone. Of course, the importance of the phonon umklapp is readily apparent even in the one-plane-wave approximation.

Although there has been no attempt to develop complete wave functions near two zones or at points of symmetry, we did introduce a four-plane-wave formalism to explore tentatively the situation with two (perpendicular) sets of zones. The result showed that simple superposition in the sense of Eq. (4.6) of the effect of the respective zones was the main effect but that there were smaller "coupling terms" that were of the order of 10% for this case, which involved an appreciable coupling constant.

Lastly, an iteration technique was presented for the calculation of $\tau_p(\vec{k})$ along particular symmetry directions which appears to converge, in general, very rapidly.

Of the results more specific to the particular metal parameters chosen, the most interesting was the fact that the relaxation-time tensor was nearly a scalar times the idem tensor at most $\vec{k}$. It seems to be generally true that the "nonscalar" part is particularly small near the zone, but under some circumstances may be appreciable near the "equator."

The pronounced maximum of τ_1 at the cap region seems to depend quite sensitively on the form of the $F(q)$, particularly around $(1+\gamma)k_F$. The results and experience gained in this exercise with a fictitious metal have been applied in the next paper[16] in an attack on a real polyvalent metal, zinc.

---

*Supported in part by the National Science Foundation under Grant No. GP28865.

†Work begun while a Visiting Professor at Cornell, 1968–1969.

‡Present address: Physics Department, Tamkang College of Arts and Sciences, Tamsui, Taipei Hsien, Taiwan.

[1]J. M. Ziman, *Electron and Phonons* (Oxford U. P., London, 1960); Frank J. Blatt, *Physics of Electric Conduction in Solids* (McGraw-Hill, New York, 1969); P. L. Taylor, *A Quantum Approach to the Solid State* (Prentice-Hall, Englewood Cliffs, N. J., 1970).

[2]P. B. Allen and Marvin L. Cohen, Phys. Rev. 187, 525 (1969).

[3]P. G. Klemens and J. L. Jackson, Physica (Utr.) 30, 2031 (1964).

[4]R. C. Dynes and J. P. Carbotte, Phys. Rev. 175, 913 (1968).

[5]W. E. Lawrence and J. W. Wilkins, Phys. Rev. B 6, 4466 (1972).

[6]V. Heine and M. L. Cohen, *Solid State Physics* (Academic, New York, 1970), Vol. 24.

[7]L. J. Sham and J. M. Ziman, *Solid State Physics* (Academic, New York, 1963), Vol. 15.

[8]G. Baym, Phys. Rev. 135, 1691 (1964).

[9]J. M. Ziman, Adv. Phys. 13, 89 (1964).

[10]E. Borchi, S. DeGennaro, and P. I. Taselli, Phys. Status Solidi B 46, 489 (1971).

[11]P. Pecheur and G. Toussaint, J. Phys. Chem. Solids 33, 2281 (1972).

[12]P. Pecheur and G. Toussaint, Phys. Rev. B 7, 1223 (1973).

[13]J. M. Ziman, *Electrons and Phonons* (Oxford U. P., London, 1960), Chap. IX.

[14]P. L. Taylor, Proc. R. Soc. A 275, 200 (1963); 275, 209 (1963).

[15]H. B. Huntington, W. B. Alexander, M. D. Feit, and J. L. Routbort, *Atomic Transport in Solids and Liquids*, edited by A. Lodding and T. Lagerwall (Verlag, Tubingen, Germany, 1973).

[16]W.-C. Chan and H. B. Huntington, following paper, Phys. Rev. B 12, 5441 (1975).

[17]M. D. Feit and H. B. Huntington, Phys. Rev. B 5, 1416 (1972). The paper is I in this NFEM series.

[18]B. O. Pierce, *Short Table of Integrals*, No. 300 (Ginn, Boston, 1929).

[19]Reference 7, pp. 223–227.

[20]J. M. Ziman, Phys. Rev. 121, 1320 (1961).

[21]H. B. Huntington and W.-C. Chan, Report No. 2118, issued by the Materials Science Center, Cornell University, Ithaca, N. Y. (unpublished).